Micro-Macroscopic Coupled Modeling of Batteries and Fuel Cells

I. Model Development

C. Y. Wang* and W. B. Gu

Department of Mechanical Engineering and Pennsylvania Transportation Institute, The Pennsylvania State University, University Park, Pennsylvania 16802, USA

B. Y. Liaw*

Hawaii Natural Energy Institute, University of Hawaii at Manoa, Honolulu, Hawaii 96822, USA

ABSTRACT

A micro-macroscopic coupled model, aimed at incorporating solid-state physics of electrode materials and interface morphology and chemistry, has been developed for advanced batteries and fuel cells. Electrochemical cells considered consist of three phases: a solid matrix (electrode material or separator), an electrolyte (liquid or solid), and a gas phase. Macroscopic conservation equations are derived separately for each phase using the volume averaging technique and are shown to contain interfacial terms which allow for the incorporation of microscopic physical phenomena such as solid-state diffusion and ohmic drop, as well as interfacial phenomena such as phase transformation, precipitation, and passivation. Constitutive relations for these interfacial terms are developed and linked to the macroscopic conservation equations for species and charge transfer. A number of nonequilibrium effects encountered in high-energy-density and high-power-density power sources are assessed. Finally, conditions for interfacial chemical and electrical equilibrium are explored and their practical implications are discussed. Simplifications of the present model to previous macrohomogeneous models are examined. In a companion paper, illustrative calculations for nickel-cadmium and nickel-metal hydride batteries are carried out. The micro-macroscopic model can be used to explore material and interfacial properties for desired cell performance.

Introduction

Electrochemical power sources such as lead-acid, nickel-cadmium (Ni–Cd), nickel–metal hydride (Ni–MH), and lithium batteries, as well as various fuel cells, are widely used in consumer applications and electric vehicles. These and future applications place an ever-increasing demand for developing more advanced power sources with higher energy density, higher power density, and longer cycle life. Mathematical modeling is indispensable in this development process, because a cell model, once validated experimentally, can be used to identify cell-limiting mechanisms and forecast cell performance for design, scale-up, and optimization. Modeling and simulation of battery and fuel-cell systems has been a rapidly expanding field, thanks in part to the advent of high-performance computers and advanced numerical algorithms.[1] Comprehensive models are frequently employed to study such battery cells as lead-acid,[2-5] nickel-cadmium,[6-9] nickel–metal hydride,[10] and lithium-ion,[11] single electrodes such as metal hydrides,[12,13] and fuel cells such as molten-carbonate[14,15] and proton-exchange-membrane[16,17] systems. The objective of the present work is to develop a new modeling framework to rigorously and systematically integrate microscopic and interfacial phenomena into a macroscopic battery or fuel-cell electrode model.

The majority of advanced battery and fuel-cell systems employ porous electrodes because they provide large surface areas and a close proximity of the pore electrolyte or gas (in fuel cells) to the electrode material to facilitate electrochemical reactions.[1] A porous electrode cell consists of three phases: a solid matrix, an electrolyte, and a gas phase, with complex interfacial structures. In order to accurately capture the dynamic cell behavior, it is important not only to consider species and charge transfer across the cell but also account for a variety of microscopic phenomena occurring inside the active material as well as on the electrolyte/electrode interface. These microscopic and interfacial phenomena largely control the rate of electrochemical reactions and hence battery performance and lifetime, particularly in high-energy-density and high-power-density situations. For instance, in nickel–metal hydride batteries, proton diffusion in the active material of nickel electrodes and hydrogen diffusion in metal hydride particles are found to be the primary factors limiting battery performance and active material utilization.[8,12,18,19]

For lead-acid batteries under extremely high current and short pulse discharge, LaFollette and Bennion[20] found that the acid concentration at the electrode/electrolyte interface significantly deviates from that within the pore electrolyte, and interface passivation occurs as a result of $PbSO_4$ crystal nucleation and growth. These and other nonequilibrium phenomena occurring at the microscale can have strong implications for the cell discharge and charge curves in high-power and short-pulse applications.[21,22]

It is usually impossible to solve the exact equations on a microscopic scale due to the complex interface morphology. Instead, macroscopic cell models are derived by averaging the microscopic (exact) equations over a representative elementary volume that contains all phases. This volume is much smaller than the cell size but large compared to the pore size of the electrode. Phase-interaction terms appear in the resulting macroscopic equations that physically represent the effects of the morphology and chemistry of an interface as well as microscopic transport phenomena on both sides of the interface. Unfortunately, in the current literature these phase-interaction terms have been either ignored or simplified using equilibrium assumptions to obtain macrohomogeneous battery[23] and fuel-cell[15] models. In other words, the interfacial quantities, which are important for determining the electrochemical reaction rates, such as species concentrations and electrical potentials at the electrode/electrolyte interface, were not distinguished from their phase-averaged counterparts and thus the nonequilibrium effects on the cell performance cannot be assessed.

Most recently, efforts have been made to modify macrohomogeneous models in order to accommodate nonequilibrium effects occurring at the electrode/electrolyte interface and solid-state diffusion in active materials of intercalative electrodes. Notably, LaFollette and Bennion[20] integrated two ad hoc submodels for the acid concentration variation within electrode pores and interface passivation due to $PbSO_4$ precipitation in order to predict experimental discharge of a lead-acid cell at high rates and short pulses. Fuller et al.[11] introduced a microscopic diffusion equation to describe the insertion of lithium ions into the cathode material. An analytical solution to this equation obtained by the method of superposition was then incorporated into a macrohomogeneous model to predict lithium/polymer cell behavior.

* Electrochemical Society Active Member.

Similarly, Bouet et al.[18] and De Vidts and White[9] accounted for microscopic diffusion and ohmic drop occurring inside the active material of a nickel electrode but using a pseudo two-dimensional numerical approach. In this approach, a pseudo dimension is defined inside the layer of active material from the nickel substrate to the interface with the electrolyte. Differential equations were then solved numerically in the physical dimensions as well as along this added "microscopic" dimension. Thus, the pseudo two-dimensional approach suffered from excessive computational burdens. Similar approaches have been applied to simulate single metal hydride electrodes[12,13] and a Ni–MH cell.[10]

The present work builds upon previous work by using the volume-averaging technique for the derivation of cell models,[1,15,23,31] and places new emphasis on a detailed description of the phase-interaction terms under interfacial nonequilibrium conditions. Such a micro-macroscopic coupled model is expected to better capture the dynamic behavior of high-energy-density and high-power-density electrochemical power sources. In a companion paper, some capabilities of the micro-macroscopic model will be demonstrated through applications to Ni–Cd and Ni–MH cells.

A Micro-Macroscopic Model

Consider an electrochemical cell composed of a positive electrode, a negative electrode, and a separator in between acting as an electronic insulator, as schematically illustrated in Fig. 1. All three components are porous and wholly or partially filled with an electrolyte (either liquid or solid). The electrolyte is an electronic insulator but a good conductor of the ionic species inside the cell. In many situations, a gas phase is also present in the cell, e.g., in valve-regulated lead-acid (VRLA) batteries as well as in Ni–Cd and Ni–MH batteries during overcharge or overdischarge. Therefore, the electrochemical cell under consideration consists of three phases: solid electrode matrix (s), electrolyte (e), and gas (g). During discharge or charge, electrochemical reactions occur at the electrode/electrolyte interface (i.e., the s–e interface) according to the following general formula

$$\sum_{\text{species}} s_j M_j^z = n_j e^- \qquad [1]$$

where the summation is over all species involved in reaction j. M_j is a general symbol for the chemical formula of a species participating in the electrochemical reaction, z and s are the charge number and the stoichiometric coefficient of the species, and n is the number of electrons transferred in reaction j. The values of s_j, z, and n_j can readily be determined by comparing a specific electrode reaction to this general form.

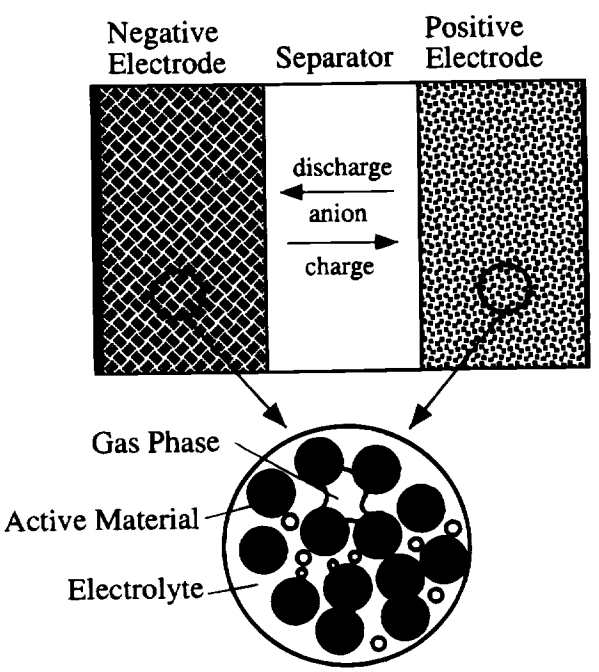

Fig. 1. Schematic illustration of the averaging volume for a battery cell.

Multiple electrochemical reactions are considered in the present work. This feature is important for the modeling of battery overcharge or overdischarge wherein side reactions such as oxygen evolution and recombination can occur along with the main electrode reactions. The production rate of a species due to electrochemical reactions occurring at the electrode/electrolyte interface is given by Faraday's law

$$r_{se} = -\sum_j \left(\frac{s_j}{n_j F} i_{nj} \right) \qquad [2]$$

with

$$i_{nj} = i_{oj} \left[\exp\left(\frac{\alpha_{aj} F}{RT} \eta_j \right) - \exp\left(-\frac{\alpha_{cj} F}{RT} \eta_j \right) \right] \qquad [3]$$

where i_{nj} is the transfer current density of reaction j, F Faraday's constant, R the universal gas constant, and T the cell temperature. Equation 3, commonly known as the Butler–Volmer equation, describes a large class of electrode reactions.

The exchange current density for reaction j, i_{oj}, depends strongly on the compositions and temperature of the electrolyte adjacent to the electrode/electrolyte interface. The anodic and cathodic transfer coefficients, α_{aj} and α_{cj}, are usually determined from experimental measurements. The surface overpotential for reaction j, η_j, is defined as

$$\eta_j = \phi_s - \phi_e - U_j \qquad [4]$$

where ϕ_s and ϕ_e are the potentials of solid electrode and electrolyte, respectively, at the electrode/electrolyte interface. The last term in Eq. 4, U_j, is the open-circuit potential of reaction j which is, in turn, a function of the reactant and product concentrations at the interface as generally expressed by the Nernst equation with respect to a specified reference electrode. Note that the interfacial overpotential, η_j, represents the driving force for electrochemical reaction j. Also, all variables in the Butler–Volmer equation, Eq. 3, are evaluated at the electrode/electrolyte interface. In high-energy-density cells or under high-power operating conditions, the interfacial values may significantly depart from their bulk counterparts within the electrode pores, giving rise to local nonequilibrium effects. Incorporating such interfacial effects constitutes a major objective of this work.

In this work it is assumed that a battery cell is isothermal so that thermal effects are not considered. The electrolyte (in either liquid or solid state) is considered as a concentrated binary electrolyte; namely, it is dissociated into a cation and an anion. Hence, the theory for concentrated binary electrolytes is employed.[1] To begin with, a set of microscopic conservation equations is summarized below.

Microscopic conservation equations.—In multiphase electrochemical systems such as porous electrodes, electrochemical processes are generally governed by the principles of conservation of mass, momentum, species, and charge in each phase. These field equations are further coupled through interfacial balance conditions. In most porous electrodes, fluid motion is absent or can be neglected and, thus, the principles of mass and momentum conservation can be eliminated from model considerations. However, in the following model development, we include these balance laws in order for the model to be applicable to general electrochemical systems, including flow-through electrodes[24] or fuel cells.[25]

Conservation of mass and momentum.—The fluid motion in phase k is determined by the mass and momentum balances, which can be expressed by

$$\frac{\partial \rho_k}{\partial t} + \nabla\cdot(\rho_k \mathbf{v}_k) = 0 \qquad [5]$$

and

$$\frac{\partial}{\partial t}(\rho_k \mathbf{v}_k) + \nabla\cdot(\rho_k \mathbf{v}_k \mathbf{v}_k) = -\nabla p_k + \nabla\cdot\tau_k + \mathbf{B}_k \qquad [6]$$

respectively. Here subscript k stands for phase k, and τ and **B** are the stress tensor and body force vector, respectively. Other symbols are defined in the List of Symbols, and explanations of the continuity and momentum equations are available in fluid mechanics textbooks.

Conservation of species.—Mass balance of a species in phase k is given by

$$\frac{\partial c_k}{\partial t} = -\nabla\cdot\mathbf{N}_k \qquad [7]$$

with the jump species balance condition at the interface between phases k and m given by Slattery[26]

$$(\mathbf{N}_k - c_k\mathbf{w}_k)\cdot\mathbf{n}_k + (\mathbf{N}_m - c_m\mathbf{w}_m)\cdot\mathbf{n}_m = -r_{km} \qquad [8]$$

where c and *N* are the molar concentration and flux of the species, with subscript k or m referring to phase k or m; the vectors **w** and **n** denote the interface velocity and the normal unit vector pointing outward from the phase denoted by the subscript; and r_{km} is the production rate of the species per unit surface area at the k–m interface due to heterogeneous electrochemical reactions as determined by Eq. 2 and/or phase transformations of a nonelectrochemical nature, such as evaporation and condensation.

In general, the molar flux of a species in phase k can be written as

$$\mathbf{N}_k = -D_k\nabla c_k + \frac{t_k}{zF}\mathbf{i}_k + c_k\mathbf{v}_k \qquad [9]$$

where D_k and t_k are the diffusion coefficient and transference number of the species in phase k with respect to a reference velocity, respectively. In this work, the mass-averaged velocity of phase k, $\mathbf{v}_k$, is conveniently chosen as the reference velocity because it is a primary variable in the continuity and momentum equations, i.e., Eq. 5 and 6. Equation 9 indicates that the species transfer in phase k is due to diffusion, migration, and advection. In a solid electrolyte the solid velocity is identically zero, leaving the species transfer by diffusion and migration only. Further, migration of ionic species in solid electrode materials under an electric field is usually negligible (i.e., $t_s \approx 0$).

Conservation of charge.—Electrochemical reactions occur at the interface between the active material and the electrolyte. Therefore, no charge is generated or consumed within each phase, yielding

$$\nabla\cdot\mathbf{i}_k = 0 \qquad [10]$$

with the interface boundary condition

$$\mathbf{i}_k\cdot\mathbf{n}_k = -\sum_j i_{nj} \qquad [11]$$

where $\mathbf{i}_k$ is the current density in phase k.

The transport of charge in the solid active material is by electrons and thus can be described by Ohm's law

$$\mathbf{i}_s = -\sigma\nabla\phi_s \qquad [12]$$

where $\mathbf{i}_s$ and ϕ_s are the current density and electric potential in the solid phase, respectively, and σ is the solid electronic conductivity. In contrast, the charge transfer in electrolyte (in both liquid and solid states) is by ions that are moving due to migration and diffusion; therefore, the electrochemical potential form of Ohm's law, which includes the combined effects of concentration and potential gradients, is used for a concentrated binary electrolyte

$$\mathbf{i}_e = -\kappa\nabla\phi_e - \kappa_D\nabla(\ln c_e^i) \qquad i = + \text{ or } - \qquad [13]$$

where κ is the effective conductivity of the electrolyte and κ_D is termed as "diffusion conductivity" to account for the rate of charged particle motion due to diffusion of ionic species (under the influence of a concentration gradient). Following Newman[1] (e.g., Section 12.4), one can show that

$$\kappa_D = \frac{\nu RT\kappa}{F}\left(\frac{s_i}{n\nu_i} + \frac{t_i^o}{z_i\nu_i} - \frac{s_o c_e}{n c_o}\right)\left(1 + \frac{d\ \ln\ f_\pm}{d\ \ln\ c_e}\right) \qquad [14]$$

where n, s_+, s_-, s_o, ν_+, ν_-, and ν represent the number of electrons transferred, the stoichiometric coefficients for anion, cation, and solvent, and the numbers of cation, anion, and moles of ions into which a molecule of electrolyte dissociates in the reaction at the reference electrode, respectively; c_e and c_o are the molar concentrations of the electrolyte and solvent in the electrolyte phase, respectively, whereas c_e^i is the molar concentration of ion i. Last, $f_\pm$ is the mean molar activity coefficient of the electrolyte and t_i^o is the transference number of cation or anion with respect to the solvent velocity.

Volume averaging.—Macroscopic governing equations can be derived from their microscopic counterparts using the local volume averaging technique as demonstrated in the literature on transport in porous media.[27-30] The same technique has also been widely used in the modeling of batteries[23,31] and fuel cells.[15] Therefore, this section only briefly outlines the key averaging steps and theorems for completeness.

Let V_O be the volume of a representative elementary volume (REV) containing a solid phase (k = s) (electrode matrix), an electrolyte phase (k = e) (liquid or solid), and a gas phase (k = g). The solid phase may consist of both a substrate and an active material layer. For any quantity in phase k, Ψ_k, the general averaging theorems can be stated as[27,28,30]

Temporal derivative

$$\left\langle\frac{\partial\Psi_k}{\partial t}\right\rangle = \frac{\partial\langle\Psi_k\rangle}{\partial t} - \frac{1}{V_O}\int_{A_k}\Psi_k\mathbf{w}_k\cdot\mathbf{n}_k dA \qquad [15]$$

Spatial derivative

$$\langle\nabla\Psi_k\rangle = \nabla\langle\Psi_k\rangle + \frac{1}{V_O}\int_{A_k}\Psi_k\mathbf{n}_k dA \qquad [16]$$

where $\mathbf{w}_k$ is the velocity of the surface bounding phase k, $\mathbf{n}_k$ is the normal unit vector pointing outward from phase k, and A_k stands for the total interfacial area of the k phase adjacent to all other phases, m

$$A_k = \sum_m A_{km} \qquad m \neq k \qquad [17]$$

The averaging operator and the intrinsic volume average are defined, respectively, as

$$\langle\Psi_k\rangle = \frac{1}{V_O}\int_{V_O} X_k\Psi_k dV \qquad [18]$$

$$\langle\Psi_k\rangle^k = \frac{1}{V_k}\int_{V_O} X_k\Psi_k dV \qquad [19]$$

with X_k denoting a phase function, equal to unity in phase k and zero elsewhere, and V_k is the volume of phase k in V_O. By definition, these two volume averages are related by

$$\langle\Psi_k\rangle = \epsilon_k\langle\Psi_k\rangle^k \qquad [20]$$

where ϵ_k is the volume fraction of phase k in the averaging volume, V_O.

Macroscopic equations.—Equations 15 and 16 are the theorems needed to obtain a set of macroscopic equations by volume-averaging the microscopic governing equations. A detailed derivation follows with particular focus on the treatment of newly arising phase interaction terms so that a closed micro-macroscopic model is obtained.

Equation of mass conservation.—Applying the averaging procedure to Eq. 5 and making use of the theorems, Eq. 15 and 16, yields[32]

$$\frac{\partial(\epsilon_k\rho_k)}{\partial t} + \nabla\cdot(\epsilon_k\rho_k\langle\mathbf{v}_k\rangle^k) = \sum_m \Gamma_{km} \qquad m \neq k \qquad [21]$$

with

$$\Gamma_{km} = \frac{1}{V_O}\int_{A_{km}} \rho_k(\mathbf{w}_k - \mathbf{v}_k)\cdot\mathbf{n}_k dA \qquad [22]$$

Here Γ_{km} represents the phase transformation rate at the k–m interface from phase m to phase k. Using the mean value theorem for integrals, this interfacial term can be modeled as a product of a specific interfacial area and a mean interfacial flux, namely

$$\Gamma_{km} = a_{km}\rho_k\overline{w}_{nkm} \qquad [23]$$

where $a_{km} = A_{km}/V_O$ is the specific area (cm^2/cm^3) of the k–m interface within the averaging volume, V_O, and $\overline{w}_{nkm}$ is defined as the average normal velocity of the k–m interface relative to phase k and directing outward from phase k. In the context of porous electrodes, $\overline{w}_{nkm}$ stems from the phase transformation accompanying all electrode reactions. One example is the solid/solid phase transformation, such as Pb to $PbSO_4$ and PbO_2 to $PbSO_4$ in discharge of lead-acid batteries and Cd to $Cd(OH)_2$ in Ni–Cd batteries. Another example of the interface movement can be found in hydriding and dehydriding processes of metal hydride alloys.

At the electrochemically active surface, i.e., the s–e interface, the interface movement leading to electrode structural changes is caused by species transformation during all electrochemical reactions. Hence

$$\overline{w}_{nse} = \sum_j \sum_{species}\left(\frac{s_j}{n_jF}\bar{i}_{nj}\overline{V}_s\right) \qquad [24]$$

where $\bar{i}_{nj}$ is the average transfer current density of reaction j as determined by Eq. 3 based on the average overpotential, $\bar{\eta}_j = \bar{\phi}_{se} - \bar{\phi}_{es} - U_j$, and $\overline{V}_s$ is the partial molar volume of a species in the solid phase. Substitution into Eq. 23 results in

$$\Gamma_{se} = a_{se}\rho_s\sum_j\sum_{species}\left(\frac{s_j}{n_jF}\bar{i}_{nj}\overline{V}_s\right) \qquad [25]$$

Applying Eq. 21 to the solid electrode phase (k = s) and noting that the solid velocity is zero result in

$$\frac{\partial(\epsilon_s\rho_s)}{\partial t} = a_{se}\rho_s\sum_j\sum_{species}\left(\frac{s_j}{n_jF}\bar{i}_{nj}\overline{V}_s\right) \qquad [26]$$

where the partial molar volume, $\overline{V}_s$, is equal to (M_r/ρ), with M_r and ρ being the molecular weight and density of the species in the solid phase, respectively. In view of the fact that the electrode porosity is simply equal to $(1 - \epsilon_s)$, Eq. 26 is commonly used to calculate the electrode porosity variation during charge and discharge.[4,8]

Equation of momentum conservation.—Application of volume averaging to Eq. 6 results in

$$\frac{\partial}{\partial t}(\epsilon_k\rho_k\langle\mathbf{v}_k\rangle^k) + \nabla\cdot(\epsilon_k\rho_k\langle\mathbf{v}_k\rangle^k\langle\mathbf{v}_k\rangle^k) = -\epsilon_k\nabla\langle p_k\rangle^k + \nabla\cdot(\langle\tau_k\rangle + \langle\tau_k^t\rangle) + \epsilon_k\langle\mathbf{B}_k\rangle^k + \sum_m (M_{km}^d + M_{km}^\Gamma) \qquad [27]$$

with

$$\langle\tau_k^t\rangle = \langle(\mathbf{v}_k - \langle\mathbf{v}_k\rangle^k)(\mathbf{v}_k - \langle\mathbf{v}_k\rangle^k)\rangle \qquad [28]$$

$$M_{km}^d = \frac{1}{V_O}\int_{A_{km}}\tau_k\cdot\mathbf{n}_k dA \qquad [29]$$

$$M_{km}^\Gamma = \frac{1}{V_O}\int_{A_{km}}\rho_k\mathbf{v}_k(\mathbf{w}_k - \mathbf{v}_k)\cdot\mathbf{n}_k dA \qquad [30]$$

Here, $\langle\tau_k^t\rangle$ is the dispersive shear stress and M_{km}^d and M_{km}^Γ are the interfacial momentum transfer rates due to viscous/form drag and interface movement, respectively. The combined macroscopic and dispersive shear stresses in Eq. 27 can be further modeled by introducing an effective viscosity[33]

$$\langle\tau_k\rangle + \langle\tau_k^t\rangle = \mu_k^*\epsilon_k\nabla\langle\mathbf{v}_k\rangle^k \qquad [31]$$

where μ_k^* represents an overall macroscopic transport property, which is a function of not only the microscopic transport property but also the microstructure and microscopic flow fields in porous electrodes. Since flow-through electrodes are usually very slow, the effective viscosity can be taken to be equal to its microscopic counterpart as a first approximation.

In porous-media literature, the total interfacial drag, including both M_{km}^d and M_{km}^Γ, is usually modeled by introducing the generalized Darcy's law[29,34] so that

$$\sum_m (M_{km}^d + M_{km}^\Gamma) = -\epsilon_k^2\frac{\mu_k}{Kk_{rk}}\cdot\langle\mathbf{v}_k\rangle^k \qquad [32]$$

where K is the absolute permeability of the porous electrode and k_{rk} is the relative permeability for phase k which accounts for a decrease in the effective flow cross section due to the presence of other fluids in the open pores of an electrode. The relative permeability is a function of phase volume fractions as determined empirically.[30]

Substitution of Eq. 31 and 32 into Eq. 27 yields the following form of the macroscopic momentum equation

$$\frac{\partial}{\partial t}(\epsilon_k\rho_k\langle\mathbf{v}_k\rangle^k) + \nabla\cdot(\epsilon_k\rho_k\langle\mathbf{v}_k\rangle^k\langle\mathbf{v}_k\rangle^k) = -\epsilon_k\nabla\langle p_k\rangle^k + \nabla\cdot(\mu_k^*\epsilon_k\nabla\langle\mathbf{v}_k\rangle^k) + \epsilon_k\langle\mathbf{B}_k\rangle^k - \epsilon_k^2\frac{\mu_k}{Kk_{rk}}\cdot\langle\mathbf{v}_k\rangle^k \qquad [33]$$

Further assuming a constant porosity of the electrode, this equation reduces to the one previously used in the modeling of acid stratification in lead-acid batteries.[5]

Equation of species conservation.—Carrying out the same averaging procedure to Eq. 7 results in

$$\frac{\partial\langle c_k\rangle}{\partial t} = -\nabla\cdot\langle\mathbf{N}_k\rangle - \frac{1}{V_O}\int_{A_k}(\mathbf{N}_k - c_k\mathbf{w}_k)\cdot\mathbf{n}_k dA \qquad [34]$$

In view of Eq. 9, the volume-averaged molar flux of a species in phase k, $\langle\mathbf{N}_k\rangle$, can be expressed as

$$\langle\mathbf{N}_k\rangle = -\langle D_k\nabla c_k\rangle + \frac{t_k}{zF}\langle\mathbf{i}_k\rangle + \langle c_k\mathbf{v}_k\rangle \qquad [35]$$

where the coefficient t_k/zF has been removed from the averaging symbol because it can be safely assumed to be constant within the averaging volume V_O. Physically, the first term on the right side of Eq. 35 describes the macroscopic species diffusion and thus is traditionally modeled using an effective mass diffusivity,[15,23] namely

$$\langle D_k\nabla c_k\rangle = D_k^{eff}\nabla\langle c_k\rangle^k \qquad [36]$$

where D_k^{eff} also includes the effect of tortuosity. The third term on the right side of Eq. 35 is traditionally described by the product of the volume-averaged concentration and velocity plus an additional term called hydrodynamic dispersion, which results from variations of the microscopic velocity and species concentration,[30] namely

$$\langle c_k\mathbf{v}_k\rangle = \epsilon_k\langle c_k\rangle^k\langle\mathbf{v}_k\rangle^k - D_a\nabla\langle c_k\rangle^k \qquad [37]$$

where D_a is the dispersion coefficient representing the effect of axial dispersion due to the fluid flow near the pore wall differing from the bulk flow. The dispersion coefficient is not a fundamental transport property; rather, it depends on the extent of fluid mixing and vanishes in the absence of convective fluid motion.[1]

Substituting Eq. 36 and 37 into Eq. 35 results in

$$\langle \mathbf{N}_k \rangle = -(D_k^{\text{eff}} + D_a)\nabla\langle c_k \rangle^k + \frac{t_k}{zF}\langle \mathbf{i}_k \rangle + \epsilon_k \langle c_k \rangle^k \langle \mathbf{v}_k \rangle^k \quad [38]$$

so that Eq. 34 becomes

$$\frac{\partial(\epsilon_k\langle c_k\rangle^k)}{\partial t} + \nabla\cdot(\epsilon_k\langle c_k\rangle^k\langle \mathbf{v}_k\rangle^k) = \nabla\cdot[D_k^{\text{eff}} + D_a)\nabla\langle c_k\rangle^k] - \nabla\cdot\left(\frac{t_k}{zF}\langle \mathbf{i}_k\rangle\right) + \frac{1}{V_O}\int_{A_k} D_k \nabla c_k\cdot\mathbf{n}_k dA - \frac{1}{V_O}\int_{A_k}\left(\frac{t_k}{zF}\right)\mathbf{i}_k\cdot\mathbf{n}_k dA + \frac{1}{V_O}\int_{A_k} c_k(\mathbf{w}_k - \mathbf{v}_k)\cdot\mathbf{n}_k dA \quad [39]$$

Application of the averaging procedure to Eq. 10 leads to

$$\nabla\cdot\langle \mathbf{i}_k\rangle + \frac{1}{V_O}\int_{A_k}\mathbf{i}_k\cdot\mathbf{n}_k dA = 0 \quad [40]$$

Thus, a part of the second term on the right side of Eq. 39 cancels out with the fourth term, and the resultant equation can be written as

$$\frac{\partial(\epsilon_k\langle c_k\rangle^k)}{\partial t} + \nabla\cdot(\epsilon_k\langle c_k\rangle^k\langle \mathbf{v}_k\rangle^k) = \nabla\cdot[D_k^{\text{eff}} + D_a)\nabla\langle c_k\rangle^k] + \sum_m (J_{km}^d + J_{km}^\Gamma) - \langle \mathbf{i}_k\rangle\cdot\nabla\left(\frac{t_k}{zF}\right) \quad [41]$$

where

$$J_{km}^d = \frac{1}{V_O}\int_{A_{km}} D_k \nabla c_k\cdot\mathbf{n}_k dA \quad [42]$$

$$J_{km}^\Gamma = \frac{1}{V_O}\int_{A_{km}} c_k(\mathbf{w}_k - \mathbf{v}_k)\cdot\mathbf{n}_k dA \quad [43]$$

The terms J_{km}^d and J_{km}^Γ represent the interfacial transfers of a species in phase k due to microscopic diffusion and interface movement, respectively. Equation 41 states the conservation of species in a liquid or solid electrolyte solution.

The interfacial species transfer terms appearing in this equation, if properly modeled, provide ways to incorporate microscopic phenomena into a macroscopic model. Based on the mean value theorem for integrals, the species transfer term due to interface movement can be modeled as the product of the mean interfacial concentration and the interfacial mass flux

$$J_{km}^\Gamma = \bar{c}_{km}\Gamma_{km} \quad [44]$$

Likewise, the integral in Eq. 42 can be evaluated as the product of the interfacial specific area and a mean interfacial diffusive flux. Physically, this interfacial mass-transfer term describes the diffusion process caused by microscopic concentration gradients. The diffusive flux is directly proportional to its driving force, namely, the difference between the interfacial and volume-averaged concentrations of a species. The flux is inversely proportional to a so-called species diffusion length, l, which characterizes the resistance to diffusion. Hence, it follows that

$$J_{km}^d = -a_{km}D_k\frac{\partial c_k}{\partial \mathbf{n}_k}\Big|_{km} = a_{km}D_k\frac{\bar{c}_{km} - \langle c_k\rangle^k}{l_{km}} \quad [45]$$

Mathematically, the diffusion length of a species in phase k is thus defined as

$$l_{km} = \frac{\bar{c}_{km} - \langle c_k\rangle^k}{-\dfrac{\partial c_k}{\partial \mathbf{n}_k}\Big|_{km}} \quad [46]$$

where D_k refers to the diffusion coefficient of a species in phase k, and $\bar{c}_{km}$ is the area-averaged concentration of the species at the k–m interface. Figure 2 schematically illustrates the microscopic concentration distributions in the solid active material and the electrolyte phase. The interface depicted in Fig. 2 represents an infinitesimal section

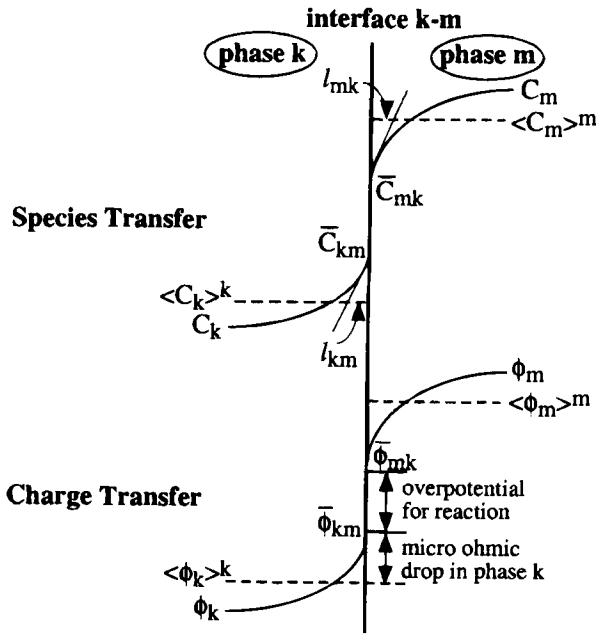

Fig. 2. Illustration of species diffusion lengths and ohmic drops.

of the interface shown in Fig. 1 and is drawn for simplicity as a straight line. The physical meaning of the diffusion length, l, is also shown. The diffusion length defined by Eq. 46 is generally a complicated function of the microscopic phenomena, and its determination requires a formal microscopic analysis of the diffusion process in a phase, as shown in the next section.

The two interfacial species transfer terms are constrained by an interfacial balance which can be obtained by integrating Eq. 8 over the interface between phase k and m within the averaging volume, V_O, yielding

$$\frac{1}{V_O}\int_{A_{km}}(-D_k\nabla c_k + \frac{t_k}{zF}\mathbf{i}_k + c_k\mathbf{v}_k - c_k\mathbf{w}_k)\cdot\mathbf{n}_k dA + \frac{1}{V_O}\int_{A_{km}}(-D_m\nabla c_m + \frac{t_m}{zF}\mathbf{i}_m + c_m\mathbf{v}_m - c_m\mathbf{w}_m)\cdot\mathbf{n}_m dA = -a_{km}\bar{r}_{km} \quad [47]$$

where $\bar{r}_{km}$ is an average reaction rate over the interface A_{km}. By the definitions given in Eq. 42 and 43 and using the relation given by Eq. 11, Eq. 47 can be rewritten as

$$(J_{km}^d + J_{km}^\Gamma) + (J_{mk}^d + J_{mk}^\Gamma) = a_{km}\left(\bar{r}_{km} - \frac{t_k + t_m}{zF}\sum_j \bar{i}_{nj}\right) \quad [48]$$

Two special cases of Eq. 48 are worth exploring. First, if the k–m interface is electrochemically reactive, the ionic species usually exists only on one side of the interface, say in phase k, so that Eq. 48 reduces to

$$(J_{km}^d + J_{km}^\Gamma) = -a_{km}\left[\sum_j\left(\frac{t_k}{zF} + \frac{s_j}{n_jF}\right)\bar{i}_{nj}\right] \quad [49]$$

where use has been made of Eq. 2 in the area-averaged sense. This expression is not only directly usable in the volume-averaged species equation, Eq. 41, but also can be used to calculate the interfacial species concentration $\bar{c}_{km}$ by substituting the constitutive relations, given by Eq. 44 and 45, into Eq. 49, yielding

$$\bar{c}_{km}\left(\Gamma_{km} + \frac{a_{km}D_k}{l_{km}}\right) = \frac{a_{km}D_k}{l_{km}}\langle c_k\rangle^k - a_{km}\left[\sum_j\left(\frac{t_k}{zF} + \frac{s_j}{n_jF}\right)\bar{i}_{nj}\right] \quad [50]$$

where the phase transformation rate Γ_{km} is determined via Eq. 25. Note that Eq. 50 is tightly coupled with the Butler–

Volmer equation which calculates the transfer current density $\bar{i}_{nj}$, because the exchange current density and equilibrium potential are strong functions of the interfacial species concentration, $\bar{c}_{km}$.

Second, if the k–m interface is electrochemically nonreactive and the species is neutral (e.g., hydrogen or oxygen dissolved in the liquid phase and existing in the gas phase as well), the interfacial species balance, Eq. 48, reduces to

$$(J^{d}_{km} + J^{\Gamma}_{km}) + (J^{d}_{mk} + J^{\Gamma}_{mk}) = 0 \qquad [51]$$

Substituting Eq. 44 and 45 into Eq. 51 and solving the resultant for Γ_{km} yields

$$\Gamma_{km} = \frac{\frac{a_{km}D_k}{l_{km}}(\bar{c}_{km} - \langle c_k\rangle^k) + \frac{a_{mk}D_m}{l_{mk}}(\bar{c}_{mk} - \langle c_m\rangle^m)}{\bar{c}_{mk} - \bar{c}_{km}} \qquad [52]$$

where use has been made of the interfacial mass balance $\Gamma_{mk} = -\Gamma_{km}$. Equation 52 can be used to calculate the phase-transformation rate, provided the interfacial species concentrations $\bar{c}_{mk}$ and $\bar{c}_{km}$ are given by thermodynamic relations at the interphase boundary.

Equations of charge conservation.—The volume-average of Eq. 10 was given by Eq. 40, which can be rewritten as

$$\nabla\cdot\langle\mathbf{i}_k\rangle - \sum_m I_{km} = 0 \qquad m \neq k \qquad [53]$$

where the interfacial current per unit of volume (A/cm^3) is given by

$$I_{km} = -\frac{1}{V_O}\int_{A_{km}} \mathbf{i}_k\cdot\mathbf{n}_k dA \qquad [54]$$

Substituting Ohm's law to relate the current density with electrical potential, we have[31]

$$\nabla\cdot(\sigma^{eff}\nabla\langle\phi_s\rangle^s) + \sum_m I_{sm} = 0 \qquad m \neq s \qquad [55]$$

for the solid phase. For the electrolyte phase, Eq. 13 is instead used, resulting in

$$\nabla\cdot(\kappa^{eff}\nabla\langle\phi_e\rangle^e) + \nabla\cdot(\kappa_D^{eff}\nabla\langle\ln\, c_e^i\rangle^e) + \sum_m I_{em} = 0 \qquad m \neq e \quad [56]$$

Using a Taylor series, it is easy to prove that[31]

$$\langle\ln\, c_e^i\rangle^e = \ln\langle c_e^i\rangle^e \qquad [57]$$

Thus, Eq. 56 can be finally rewritten as

$$\nabla\cdot(\kappa^{eff}\nabla\langle\phi_e\rangle^e) + \nabla\cdot(\kappa_D^{eff}\nabla\ln\langle c_e^i\rangle^e) + \sum_m I_{em} = 0 \qquad m \neq e \quad [58]$$

The interfacial current density I_{km} at the electrode/electrolyte interface is simply equal to

$$I_{se} = -I_{es} = a_{se}\sum_j \bar{i}_{nj} \qquad [59]$$

Alternatively, for a generic k–m interface, the interfacial current density can also be modeled, similar to the interfacial species transfer term due to diffusion, by

$$I_{km} = a_{km}\frac{\bar{\phi}_{km} - \langle\phi_k\rangle^k}{R_{km}} \qquad [60]$$

where R_{km} in the unit of Ω cm^2 is defined as

$$R_{km} = \frac{\bar{\phi}_{km} - \langle\phi_k\rangle^k}{-\sigma\frac{\partial\phi_k}{\partial\mathbf{n}_k}\big|_{km}} \qquad [61]$$

and represents a characteristic ohmic resistance between phase k and the k–m interface. Equation 60 assumes that phase k is a solid so that Ohm's law is valid for relating current to potential. The expression for the interfacial current density in a liquid phase, however, needs a slight modification by taking migration into account. Hence

$$I_{km} = a_{km}\frac{\bar{\phi}_{km} - \langle\phi_k\rangle^k}{R_{km}} + a_{km}\frac{\kappa_D}{\bar{c}_{km}l_{km}}(\bar{c}_{km} - \langle c_k\rangle^k) \qquad [62]$$

where phase k is an electrolyte. Now, combining either Eq. 60 or 62 with Eq. 59, one can determine the interfacial potentials $\bar{\phi}_{se}$ and $\bar{\phi}_{es}$, which are used, in turn, to determine the interfacial overpotential for electrochemical reactions. In practice, because the solid phase is usually a good electronic conductor (i.e., large values of σ), it follows that $\bar{\phi}_{se}$ is nearly identical to $\langle\phi_s\rangle^s$. Semiconductor electrode materials, however, are an exception in which it is necessary to differentiate $\bar{\phi}_{se}$ from $\langle\phi_s\rangle^s$. In contrast, the ionic conductivities in liquids are usually low, leading to a substantial discrepancy between $\bar{\phi}_{es}$ and $\langle\phi_e\rangle^e$, especially in high current situations. This implies that it may no longer be appropriate to use $\langle\phi_e\rangle^e$ in place of $\bar{\phi}_{es}$ in the calculation of the transfer current density via the Butler–Volmer equation. Relations between the volume-averaged and interfacial potentials are schematically illustrated in Fig. 2.

Summary of model equation.—In summary, Eq. 21, 33, 41, and 55 or 56 form a complete set of macroscopic governing equations for four volume-averaged unknowns: ϵ_k, $\langle\mathbf{v}_k\rangle^k$, $\langle c_k\rangle^k$, and $\langle\phi_k\rangle^k$. These are now summarized in Table I along with the expressions for respective interfacial transfer terms. The interfacial species and charge balances also given in Table I can be used to determine the interfacial species concentrations and electrical potentials in nonequilibrium situations and hence the rates of electrode reactions via the Butler–Volmer equation. Microscopic and interfacial phenomena, reflected through the various interfacial transfer terms, are integrated into the macroscopic cell model primarily through three interfacial parameters: the specific area a_{km}, the species diffusion length l_{km}, and the ohmic resistance R_{km}. Accurate determination of these quantities is crucial and requires a formal microscopic analysis of the interface morphology, as well as the species diffusion and charge transfer in the vicinity of the interface, as shown in the following section.

Microscopic Modeling

This section presents microscopic analyses to develop relations for the three interfacial parameters that play critical roles in the micro-macroscopic coupled model. It is shown that through these constitutive relations, microscopic phenomena such as solid-state diffusion, ohmic resistance in the semiconductor state of active materials, and interfacial phenomena (e.g., electrochemical area passivation and nonequilibrium conditions) can all be incorporated into the model in a consistent manner.

Interfacial active area.—The previous section shows that the specific area of the electrode/electrolyte interface, $a_{se} = A_{se}/V_O$, is an important ingredient in the modeling of the interfacial transfer terms. From a physical point of view, the specific area contains the information regarding the geometry of an interface that is lost through the averaging process. This information plays an important part in the cell behavior and must be restored through a constitutive relation. The specific interfacial area is dependent on the morphology and dynamics of the interface. It decreases as interface passivation occurs due to solid precipitation in electrochemical reactions. The specific area of porous electrodes can be measured by the adsorption method or double-layer charging.[1]

For an electrode composed of spherical particles of radius r_s, the initial specific area is readily given by

$$a^o_{se} = \frac{3\epsilon_s}{r_s} = \frac{3(1-\epsilon_o)}{r_s} \qquad [63]$$

where ϵ_o is the porosity of the electrode. For irregularly shaped particles, it is proposed to directly base the micro-macroscopic model on the specific surface area a^o_{se} because it can be easily measured and its inverse is a more accurate representation of the length scale of a complex micro-

Table I. Summary of the micro-macroscopic model.

	Macroscopic conservation equations	Interfacial transfer terms	Interfacial balances
Mass	$\frac{\partial(\epsilon_k\rho_k)}{\partial t} + \nabla\cdot(\epsilon_k\rho_k\langle\mathbf{v}_k\rangle^k) = \sum_{m,m\neq k}\Gamma_{km}$	$\Gamma_{km} = a_{km}\rho_k\bar{w}_{nkm}$	$\Gamma_{km} + \Gamma_{mk} = 0$
Momentum	$\frac{\partial}{\partial t}(\epsilon_k\rho_k\langle\mathbf{v}_k\rangle^k) + \nabla\cdot(\epsilon_k\rho_k\langle\mathbf{v}_k\rangle^k\langle\mathbf{v}_k\rangle^k) = -\epsilon_k\nabla\langle p_k\rangle^k + \nabla\cdot(\mu_k^*\epsilon_k\nabla\langle\mathbf{v}_k\rangle^k) + \epsilon_k\langle\mathbf{B}_k\rangle^k - \epsilon_k^2\frac{\mu_k}{Kk_{rk}}\cdot\langle\mathbf{v}_k\rangle^k$		
Species	$\frac{\partial(\epsilon_k\langle c_k\rangle^k)}{\partial t} + \nabla\cdot(\epsilon_k\langle c_k\rangle^k\langle\mathbf{v}_k\rangle^k) = \nabla\cdot[(D_k^{eff} + D_a)\nabla\langle c_k\rangle^k] + \sum_{m,m\neq k}[J_{km}^d + J_{km}^\Gamma] - \langle\mathbf{i}_k\rangle\cdot\nabla\left(\frac{t_k}{zF}\right)$	$J_{km}^d = a_{km}\frac{D_k}{l_{km}}(\bar{c}_{km} - \langle c_k\rangle^k)$ $J_{km}^\Gamma = c_{km}\Gamma_{km}$	$(J_{km}^d + J_{km}^\Gamma) + (J_{mk}^d + J_{mk}^\Gamma) = a_{km}\left(\bar{r}_{km} - \frac{t_k + t_m}{zF}\sum_j \bar{i}_{nj}\right)$
Charge	$\nabla\cdot(\sigma^{eff}\nabla\langle\phi_s\rangle^s) + \sum_{m,m\neq s} I_{sm} = 0$ $\nabla\cdot(\kappa^{eff}\nabla\langle\phi_e\rangle^e) + \nabla\cdot(\kappa_D^{eff}\nabla\langle\ln c_e^1\rangle^e) + \sum_{m;m\neq e} I_{em} = 0$	$I_{sm} = a_{sm}\frac{\bar{\phi}_{sm} - \langle\phi_s\rangle^s}{R_{sm}}$ $I_{em} = a_{em}\frac{\bar{\phi}_{em} - \langle\phi_e\rangle^e}{R_{em}} + a_{em}\frac{\kappa_D}{\bar{c}_{em}l_{em}}(\bar{c}_{em} - \langle c_e\rangle^e)$	$I_{sm} + I_{ms} = 0$ $I_{em} + I_{me} = 0$

Supplemental relations for the electrode/electrolyte interface

Average normal velocity	$\bar{w}_{nse} = \sum_j\sum_{species}\left(\frac{s_j}{n_jF}\bar{i}_{nj}\bar{V}_s\right)$
Average reaction rate	$\bar{r}_{se} = -\sum_j\left(\frac{s_j}{n_jF}\bar{i}_{nj}\right)$
Average transfer current	$\bar{i}_{nj} = i_{oj}\left[\exp\left(\frac{\alpha_{aj}F}{RT}(\bar{\phi}_{se} - \bar{\phi}_{es} - U_j)\right) - \exp\left(-\frac{\alpha_{cj}F}{RT}(\bar{\phi}_{se} - \bar{\phi}_{se} - U_j)\right)\right]$

structure than traditionally employed average particle sizes.[35,36]

Interface passivation may occur as a result of nucleation and growth of solid precipitates; for example, in lead-acid batteries the solid $PbSO_4$ crystals nucleate and grow during discharge, passivating a portion of the interfacial area that would otherwise be available for electrochemical reactions. The passivation in this case can be commonly described by a simple geometric relation[20]

$$a_{se} = a_{se}^o[1 - (\epsilon_{PbSO_4}/\epsilon_o)^p] \quad [64]$$

where ϵ_{PbSO_4} is the volume fraction of $PbSO_4$ precipitate and p is a geometrical factor varying from 0 to 1. Small values of p are indicative of flat, plate-like precipitate of $PbSO_4$ crystals, which in the limit of infinitely small p values become a sheet of precipitate. Larger values of p suggest needle-like crystals which block little active area. The volume fraction ϵ_{PbSO_4} can further be calculated by combining the nucleation and growth models of $PbSO_4$ crystals, as done by LaFollette and Bennion.[20] An alternative but simpler approach is to correlate the ratio $\epsilon_{PbSO_4}/\epsilon_o$ with the depth of discharge

$$\frac{\epsilon_{PbSO_4}}{\epsilon_o} = \frac{Q}{Q_o} \quad [65]$$

where Q_o is the maximum capacity of the electrode (C/cm^3) and Q is the number of coulombs of charge remaining.

Interface passivation of metal hydride (MH) particles in an MH electrode has been experimentally noted to cause slow degradation in the performance of the MH electrode upon cycling;[37] however, no modeling work has been carried out on the effect of this passivation on battery performance.

Species diffusion length.—Here we derive analytical expressions for the species diffusion length in all three geometries of interest: plate-like, cylindrical, and spherical. The cylindrical geometry is representative of the morphology of the nickel electrode in Ni–Cd and Ni–MH batteries, while a sphere is typical of the morphology of many particulate electrodes such as MH and lithium composite electrodes. Take the cylindrical geometry as an example. The active materials are assumed to be uniformly coated onto a cylindrical substrate. Because the layer of active materials is thin, the effect of curvature may be insignificant and it is reasonable to assume a parabolic distribution for the species concentration across the layer,[38] namely

$$c_s = a_0 + a_1 r + a_2 r^2 \quad [66]$$

where r is the radial distance. The following boundary conditions apply

$$\frac{\partial c_s}{\partial r} = 0 \text{ at } r = r_o \quad [67]$$

$$c_s = \bar{c}_{se} \text{ at } r = r_s \quad [68]$$

where r_o is the radius of the substrate and r_s is the radius of the electrode/electrolyte interface. In addition, the known local volume-averaged concentration $\langle c_s\rangle^s$ is defined as

$$\langle c_s \rangle^s = \frac{1}{V_s}\int_{V_s} c_s \, r dr = \frac{2}{r_s^2 - r_o^2}\int_{r_o}^{r_s} c_s \, r dr \qquad [69]$$

Using Eq. 67–69, the three coefficients, a_0, a_1, and a_2 in Eq. 66 can be determined, and the species concentration profile is found to be given by

$$\frac{\bar{c}_{se} - c_s}{\bar{c}_{se} - \langle c_s \rangle^s} = \frac{(r_s - r)(r_s - 2r_o + r)}{\frac{r_s^2 - r_o^2}{2} - \frac{2}{3}r_s r_o + \frac{4r_o^3}{3(r_s + r_o)}} \qquad [70]$$

According to Eq. 46, the diffusion length is readily found to be expressed by

$$l_{se} = \frac{r_s + r_o}{4} - \frac{r_s r_o}{3(r_s - r_o)} + \frac{2r_o^3}{3(r_s^2 - r_o^2)} \qquad [71]$$

When $r_o = 0$, Eq. 71 reduces to

$$l_{se} = \frac{r_s}{4} \qquad [72]$$

This clearly indicates that the diffusion length is proportional to the characteristic length of electrode particles with a numerical factor of the order of unity.

This derivation for the species diffusion length can be similarly extended to Cartesian and spherical coordinate systems. For brevity, only the final results are presented here

$$l_{se} = \frac{r_s}{3} \qquad [73]$$

for a plate-like active material layer with the half thickness of r_s and

$$l_{se} = \frac{r_s}{5} \qquad [74]$$

for a spherical particle of radius r_s. Equation 74 is useful in the modeling of MH and lithium composite electrodes, while Eq. 71 is applicable to composite nickel electrodes with substrates. Note that the diffusion lengths for various geometries differ only by a numerical factor of the order of unity. Use of diffusion lengths provides an opportunity to include, in a macroscopic cell model, the rate-limiting microscopic phenomena such as solid-state diffusion in active materials and ionic species diffusion in the electrolyte.

Microscopic ohmic resistance.—Similar to the diffusion length, the microscopic ohmic resistance defined by Eq. 61 is dependent on the charge-transport processes in a given phase and must be analyzed microscopically. Once again, the charge transfer inside a cylindrical active material layer bounded by the electrode/electrolyte and electrode/substrate interfaces is considered.

By definition (i.e., Eq. 61), the ohmic resistances from the electrode/electrolyte interface and from the electrode/substrate interface to the bulk of the active material layer are given, respectively, by

$$R_{se} = \frac{\bar{\phi}_{se} - \langle \phi_s \rangle^s}{-\sigma_s \left.\frac{\partial \phi_s}{\partial r}\right|_{r=r_s}} \qquad [75]$$

$$R_{sb} = \frac{\bar{\phi}_b - \langle \phi_s \rangle^s}{-\sigma_o \left.\frac{\partial \phi_s}{\partial r}\right|_{r=r_o}} \qquad [76]$$

where the subscript b denotes the substrate and ϕ_s is the microscopic profile of electrical potential in phase s (i.e., active material layer). Note that the conductivity σ varies with the location as it is a function of the local state of charge, so the symbols σ_o and σ_s denote the conductivities at the electrode/substrate and electrode/electrolyte interfaces, respectively. The current flows only in the radial direction and there is no charge generated or consumed within the active layer. As such, integration of charge balance over the thickness of the active material layer yields

$$\left(\sigma \cdot r \frac{\partial \phi_s}{\partial r}\right)_{r=r_o} = \left(\sigma \cdot r \frac{\partial \phi_s}{\partial r}\right)_{r=r_s} \qquad [77]$$

In addition, two other boundary conditions must be met

$$\phi_s = \phi_b \text{ at } r = r_o \text{ and } \phi_s = \bar{\phi}_{se} \text{ at } r = r_s \qquad [78]$$

Hence, assume a parabolic profile for ϕ_s

$$\phi_s = a_0 + a_1(r - r_o) + a_2(r - r_o)^2 \qquad [79]$$

where three coefficients can be determined from the three boundary conditions given in Eq. 77 and 78. Substitution of the profile for ϕ_s into Eq. 75 and 76 yields

$$R_{se} = \frac{r_s}{12}\left(\frac{r_s - r_o}{r_s + r_o}\right)\left(\frac{r_s + 3r_o}{\sigma_o r_o} + \frac{3r_s + 5r_o}{\sigma_s r_s}\right) \qquad [80]$$

and

$$R_{sb} = \frac{r_o}{12}\left(\frac{r_s - r_o}{r_s + r_o}\right)\left(\frac{5r_s + 3r_o}{\sigma_o r_o} + \frac{3r_s + r_o}{\sigma_s r_s}\right) \qquad [81]$$

Clearly, these resistances are directly proportional to a microlength scale (r_s or r_o) and inversely proportional to the conductivity σ, thus characterizing the microscopic ohmic drop occurring inside the active material of the electrode.

Discussion

The model equations developed in the preceding section and summarized in Table I are valid for any volume fraction and in both electrode and separator regions. They even reduce to the correct limit for a pure liquid electrolyte reservoir (i.e., $\epsilon_e = 1$). Therefore, the present model is suitable for one-domain numerical solution methodologies, which remove typical difficulties associated with traditional multidomain approaches where matching boundary conditions between subdomains must be implemented. This feature can facilitate numerical implementation and simulation of complete cells.

We explore the limiting conditions with regard to interfacial equilibrium and associated physical significance in the following section. Reduced versions of the present model in the equilibrium case are then derived and compared to previous macrohomogeneous models for batteries and fuel cells.

Interfacial chemical equilibrium.—According to Eq. 50 or 52, interfacial chemical equilibrium (i.e., $\bar{c}_{km} = \langle c_k \rangle^k$) requires that

$$\frac{a_{km} D_k}{l_{km}} \to \infty \qquad [82]$$

Recognizing that $a_{km} \sim 1/r_s$ and $l_{km} \sim r_s$ (see Eq. 63 and 72–74), the condition given by Eq. 82 can equivalently be expressed as

$$\frac{D_k}{r_s^2} \to \infty \qquad [83]$$

For typical liquid-mass diffusivities and particle sizes of battery electrodes, Eq. 83 is generally satisfied except in high-current and/or short-pulse situations. In contrast, species diffusion coefficients in solids are usually four to six orders of magnitude lower than that of liquids and, thus, the condition expressed by Eq. 83 is highly questionable, implying that the solid-state diffusion is likely to be a limiting mechanism for cell behavior. The interfacial chemical nonequilibrium in the solid active material phase has long been recognized and extensively studied.

Moreover, note that the left side of Eq. 83 represents the inverse of the characteristic time for species diffusion from the electrochemical interface into the interior of each solid particle or electrolyte-occupied pore. For a pore size of 1–10 μm and an effective diffusion coefficient of 10^{-9} m^2/s in common liquid electrolytes, this leads to diffusion times on the order of 1–100 ms. In rapidly pulsed charge and discharge situations wherein pulses are usually of 1 ms duration, the interfacial chemical equilibrium inside electrolyte pores within an averaging volume is clearly invalid. For a solid-phase electrolyte (e.g., in lithium/poly-

mer batteries), the diffusion coefficient is on the order of 10^{-11} m^2/s [39,40] and the corresponding diffusion times would increase up to between 100 ms and 10 s. In this case, the interfacial chemical equilibrium in solid-phase electrolyte becomes questionable even under normal discharge and recharge conditions. A scenario of relevance is the electric vehicle application in which batteries are tested using such standard procedures as dynamic stress test (DST) and simplified federal urban driving schedule (SFUDS) in which the discharge peak occurs over a period of only 8 s.

Interfacial electrical equilibrium.—Likewise, according to Eq. 60 or 62, the condition for interfacial electric equilibrium (i.e., $\bar{\phi}_{km} = \langle\phi_k\rangle^k$) can be stated as

$$\frac{a_{km}}{R_{km}} \to \infty \qquad [84]$$

or

$$\frac{\sigma}{r_s^2} \text{ or } \frac{\kappa}{r_s^2} \to \infty \qquad [85]$$

for the solid active material and electrolyte, respectively. Clearly, a large conductivity and a small pore size would support the electrical equilibrium at the electrode/electrolyte interface. The left side of Eq. 85 represents the inverse of a volume resistance (Ω cm^3), the physical significance of which can be explained by the Wagner number[41] based on the microscopic length scale. We can define the *Wa* number as the ratio of the interfacial electrochemical kinetics resistance, R_k, to the microscopic ohmic resistance across the active material particles or the electrolyte-occupied pores, R_{km}

$$Wa = \frac{R_k}{R_{km}} \sim \frac{(\sigma \text{ or } \kappa)(\partial\eta/\partial i_n)}{r_s} \qquad [86]$$

where the characteristic kinetics resistance is taken as the tangent to the polarization curve described by the Butler–Volmer equation. Apparently, *Wa*, defined by Eq. 86, is a quantitative measure of the relative magnitude of interfacial electrical nonequilibrium as compared to the kinetic surface overpotential; in other words, for $Wa \ll 1$, interfacial potential nonequilibrium would become too significant to be neglected.

In high-current situations, Tafel kinetics is a good approximation and so Eq. 86 for the electrolyte phase can be simplified to

$$Wa = \left(\frac{RT}{\alpha F}\right)\left(\frac{\kappa}{i_n r_s}\right) \qquad [87]$$

where the first term is roughly a constant (approximately equal to 0.026 V^{-1} at room temperature) and thus the second term controls the magnitude of *Wa*. Furthermore, noting that the transfer current density, i_n, is related to the cell current density, i, through a geometrical factor, i.e., $a_{km} i_n \sim i/L_e$ as can be seen from Eq. 55 and 59, one can then recast Eq. 87 as

$$Wa = \left(\frac{RT}{\alpha F}\right)\left(\frac{\kappa L_e}{i r_s^2}\right) \qquad [88]$$

which is the ratio of the volume interfacial kinetics resistance ($RTL_e/\alpha Fi$) to the volume ohmic resistance (r_s^2/κ) appearing in Eq. 85 characterizing interfacial electrical equilibrium. It is clear from Eq. 88 that *Wa* is smaller than unity in cases of resistive electrolytes and/or high current densities, indicative of the significance of the microscopic ohmic drop in the vicinity of the interface. For a typical battery electrode with the particle size $r_s \sim 10$ μm and the electrode thickness $L_e \sim 1$ mm, *Wa* is then dependent only on the conductivity and current density. For lead-acid batteries where the ionic conductivity in the electrolyte is around 10^{-2} S/cm, *Wa* is estimated to be less than 0.026 for current densities up to 1 A/cm^2. This shows that interfacial electric equilibrium is usually a good assumption in aqueous-electrolyte batteries. However, for solid-phase electrolytes suh as those used in plastic lithium-ion batteries, the electrolyte conductivity is on the order of 10^{-3} S/cm,[40] and hence, *Wa* is equal to 0.26 for the current density of 1 A/cm^2. As such, the electrical equilibrium on the electrolyte side of the electrode/electrolyte interface may break down. Likewise, in semiconductor active materials (e.g., NiOOH), the solid conductivity can be as low as 10^{-5} S/cm and so *Wa* is about 26 in this case for the current density of 1 A/cm^2. Clearly, the microscopic ohmic drop in semiconductor active materials is not negligible and must be considered in cell models.

For thin-film batteries where L_e is less than 0.1 mm,[20,42] the threshold of current densities for interfacial electrical nonequilibrium becomes as low as 1 A/cm^2 for aqueous electrolytes and 0.1 A/cm^2 for solid-phase polymer electrolytes, respectively. These are common conditions encountered in practice.

Macrohomogeneous models.—In this subsection, we show how the present model reduces to previous macrohomogeneous models under interfacial chemical and electrical equilibrium. Two scenarios are examined separately. One is that the ionic species exists only in one phase (either solid electrode material or electrolyte), so that the macroscopic species and charge conservation equations are given by Eq. 41 along with the interfacial balance given by Eq. 49. Combination of the two equations leads to

$$\frac{\partial(\epsilon_k\langle c_k\rangle^k)}{\partial t} + \nabla\cdot(\epsilon_k\langle c_k\rangle^k\langle \mathbf{v}_k\rangle^k) = \nabla\cdot[D_k^{\text{eff}} + D_a)\nabla\langle c_k\rangle^k] - a_{se}\left(\sum_j \frac{s_j}{n_j F}\bar{i}_{nj}\right) - \nabla\cdot\left(\frac{t_k}{zF}\langle \mathbf{i}_k\rangle\right) \qquad [89]$$

where $\langle \mathbf{i}_k\rangle$ is the superficial current density through phase k, and the interfacial transfer current density $\bar{i}_{nj}$ is evaluated via the Butler–Volmer equation using the volume-averaged concentration $\langle c_k\rangle^k$ and potential $\langle\phi_k\rangle^k$ because interfacial chemical and electrical equilibrium holds true. Similarly, the macroscopic charge-balance equations can be rewritten as

$$\nabla\cdot(\sigma^{\text{eff}}\nabla\cdot\langle\phi_s\rangle^s) + a_{se}\sum_j \bar{i}_{nj} = 0 \qquad [90]$$

and

$$\nabla\cdot(\kappa^{\text{eff}}\nabla\langle\phi_e\rangle^e) + \nabla\cdot(\kappa_D^{\text{eff}}\nabla \ln\langle c_e^j\rangle^e) - a_{se}\sum_j \bar{i}_{nj} = 0 \qquad [91]$$

for the solid and solution phases, respectively. Equations 89 through 91 constitute a complete set of governing equations for three unknowns: species concentration $\langle c_k\rangle^k$, solid potential $\langle\phi_s\rangle^s$, and electrolyte potential $\langle\phi_e\rangle^e$, whereas the interfacial transfer current density is calculated by the Butler–Volmer equation as a function of $\langle c_k\rangle^k$, $\langle\phi_s\rangle^s$, and $\langle\phi_e\rangle^e$. The superficial current density is determined in terms of either potential gradient in phase k or the interfacial transfer current density. This mathematical system is the basis for previous macrohomogeneous models for a wide variety of battery systems.

In many fuel-cell systems, the species exists both in the electrolyte as a charged ion and in the gas phase as a neutral species. One can then add up the macroscopic conservation equations for the electrolyte and gas phases and make use of the interfacial balance to obtain the following

$$\frac{\partial(\epsilon_e\langle c_e\rangle^e)}{\partial t} + \frac{\partial(\epsilon_g\langle c_g\rangle^g)}{\partial t} = \nabla\cdot[(D_e^{\text{eff}}\nabla\langle c_e\rangle^e] + \nabla\cdot[(D_g^{\text{eff}}\nabla\langle c_g\rangle^g] - a_{se}\left(\sum_j \frac{s_j}{n_j F}\bar{i}_{nj}\right) - \nabla\cdot\left(\frac{t_e}{zF}\langle \mathbf{i}_e\rangle\right) \qquad [92]$$

where the interfacial species transfer terms between phases e and g have been canceled out and convective terms neglected for clarity. Equation 92 is general and does not require interfacial equilibrium conditions. However, in

order to render Eq. 92 for a single unknown, one must invoke the chemical equilibrium condition, i.e., $\langle c_g \rangle^g = H\langle c_e \rangle^e$, where H is a Henry's constant. Otherwise, there are too many unknowns contained in Eq. 92, i.e., $\langle c_g \rangle^g$ and $\langle c_e \rangle^e$. Prins-Jansen et al.[15] argued that without making the above-mentioned chemical equilibrium assumption, Eq. 92 can be reduced for the single variable defined as

$$\langle c \rangle = \epsilon_e \langle c_e \rangle^e + \epsilon_g \langle c_g \rangle^g \quad [93]$$

where $\langle c \rangle$ can be interpreted as the mixture concentration in both electrolyte and gas phases. However, this approach does not ultimately circumvent the problem associated with too many unknowns because one always needs to determine $\langle c_e \rangle^e$ and $\langle c_g \rangle^g$ individually from $\langle c \rangle$. Therefore, Eq. 92 along with the equilibrium condition essentially represents the macrohomogeneous theory for porous electrodes previously derived by Prins-Jansen et al.[15] for molten-carbonate fuel cells.

New features of the present model.—In comparison to the previous models for porous electrodes of batteries and fuel cells, some new features of the present model can be summarized as follows

1. In situations where the interfacial equilibrium (chemical and/or electrical) breaks down on the electrolyte side, as identified earlier in the present section, all previous macrohomogeneous models become invalid, whereas the present model provides the only model capable of distinguishing the interfacial values from their phase-averaged counterparts and therefore is able to address such nonequilibrium problems. Work is ongoing to use the present model to simulate high-current charge and discharge.

2. In cases where there exists interfacial equilibrium in the electrolyte phase but not in the solid electrode phase as occurring in most insertion batteries, the present model is, in principle, similar to previous macrohomogeneous models extended to account for solid-state diffusion, notably the Ni–Cd model of De Vidts and White,[8] the Ni–MH model of Paxton and Newman,[10] and the Li-ion models of Doyle et al.[39] and Fuller et al.[11] There is, however, a slight difference in the method of accounting for solid-state diffusion. Whereas the previous works use either numerical (e.g., Ref. 8) or analytical (Ref. 10, 11, and 39) solutions to a partial differential equation for microscopic species diffusion within solid particles, the present model used the diffusion-length concept. In the case of perfectly spherical particles, previous approaches are exact, whereas the present treatment is only approximate. However, the approximation thus introduced is quite acceptable, as demonstrated by a detailed comparative study to be reported in Part II.[43] In the case of irregularly shaped particles as found in practical systems, the previous numerical and analytical approaches become impossible, whereas the present model still gives good approximations. Computationally, the present model using the diffusion length is most economical among all the approaches, thus allowing for efficient simulation of complex discharge and charge schedules and driving cycles.

Conclusions

A micro-macroscopic coupled model of electrochemical kinetics and transport phenomena occurring in batteries and fuel cells has been developed using the technique of volume averaging. The model accounts for the effects of microscale and interfacial nonequilibrium processes on the macroscopic species and charge transfer. It is shown that solid-state diffusion, ohmic resistance in resistive active materials and electrolytes, and interface passivation can all be incorporated in the present model in a consistent manner. This ultimately allows for the integration of detailed chemistry and morphology of the electrode/electrolyte interface into a battery behavior model.

Application of the present model to Ni–Cd and Ni–MH batteries is described in detail in a companion paper.[43] Efforts are underway to apply the model to simulate high-power, rapidly pulsed discharge and charge batteries where interfacial nonequilibrium and thermal transport are prominent and operate concurrently. In addition, the present model capable of including a gas phase will be used to study fundamental mechanisms for overcharge or overdischarge through gas generation and recombination processes.

Acknowledgments

This work is supported in part by the Defense Advanced Research Projects Agency (DARPA), Tactical Technology Office, Electric Vehicle Technology Program, under cooperative agreement No. MDA972-95-2-0009.

Manuscript submitted December 3, 1997; revised manuscript received June 19, 1998.

The Pennsylvania State University assisted in meeting the publication costs of this article.

LIST OF SYMBOLS

A	total interfacial area, cm^2
a	specific interfacial area, cm^2/cm^3
$\mathbf{B}$	body force vector, N/cm^3
c_k	concentration of species in phase k, mol/cm^3
c_{km}	interfacial concentration of species in phase k at k–m interface, mol/cm^3
$\bar{c}_{km}$	area-averaged concentration of species over k–m interface, mol/cm^3
$\langle c_k \rangle^k$	volume-averaged concentration of a species over phase k, mol/cm^3
D	diffusion coefficient of species, cm^2/s
D_a	dispersion coefficient, cm^2/s
F	Faraday's constant, 96,487 C/mol
$f_\pm$	mean molar activity coefficient of the electrolyte
I	volumetric interfacial current density, A/cm^3
$\mathbf{i}_k$	current density in phase k, A/cm^2
i_{nj}	transfer current density of reaction j, A/cm^2
i_{0j}	exchange current density of reaction j, A/cm^2
J^d_{km}	interfacial species transfer rate due to diffusion, mol/cm^3 s
J^Γ_{km}	interfacial species transfer rate due to interface movement, mol/cm^3 s
K	absolute permeability of porous electrode
k_{rk}	relative permeability of phase k
L_e	thickness of electrode, cm
l_{km}	diffusion length of species from k–m interface into phase k, cm
M^z_j	symbol representing the chemical formula of species with a charge number of z in reaction j
M^d_{km}	interfacial momentum transfer rate due to diffusion, g/cm^2 s^2
M^Γ_{km}	interfacial momentum transfer rate due to interface movement, g/cm^2 s^2
M_r	molecular weight of species, g/mol
$\mathbf{n}_k$	normal unit vector pointing outward from phase k
$\mathbf{N}_k$	molar flux of species of phase k, mol/cm^2 s
n_j	number of electrons transferred in reaction j
p	pressure, Pa
Q	charge capacity of electrode, C/cm^3
Q_o	maximum charge capacity of electrode, C/cm^3
R	universal gas constant, 8.3143 J/mol K
R_{km}	electrical resistance from k–m interface to bulk of phase k, Ω cm^2
r	radial coordinate, cm
r_{km}	production rate of species at k–m interface, mol/cm^3 s
r_o	radius of cylindrical substrate, cm
r_s	radius of cylinder or sphere of electrode active material, cm
s_j	stoichiometric coefficient of species in reaction j
T	absolute temperature of the cell system, K
t	time, s
t_k	transference number of species in phase k with respect to a reference velocity
t^o_i	transference number of cation or anion with respect to the solvent velocity
U_j	open-circuit potential of reaction j, V
V_k	volume of phase k in the REV, cm^3
V_o	volume of the REV in porous medium, cm^3
$\mathbf{v}_k$	reference velocity of phase k, cm/s
Wa	Wagner number
$\bar{w}_{nkm}$	average normal velocity of the k–m interface relative to phase k, cm/s
x	x coordinate, cm
z	charge number of species

Greek

α_{aj}, α_{cj}	anodic and cathodic transfer coefficients for reaction j

ϵ_k volume fraction of phase k in the REV
ϵ_o porosity of electrode
η_j surface overpotential of electrode reaction j, V
κ conductivity of an electrolyte, S/cm
κ_D diffusion conductivity of species, A/cm
ρ density of species, g/cm^3
σ conductivity of the active material in the electrode, S/cm
μ dynamic viscosity, g cm/s
ν moles of ions into which a mole of electrolyte dissociates
ν_+, ν_- numbers of cations and anions into which a mole electrolyte dissociates
τ stress tensor, N/cm^2
ϕ_k potential in phase k, V
ϕ_{km} surface potential of phase k at k–m interface, V
$\bar{\phi}_{km}$ average surface potential of phase k over k–m interface, V
$\langle\phi_\kappa\rangle^k$ volume-averaged potential over phase k, V
Ψ_k general quantity in phase k

Subscript

b substrate
e electrolyte
g gas phase
s solid phase

Superscript

eff effective
o initial
$\overline{}$ overbar, average over interface

REFERENCES

1. J. Newman, *Electrochemical Systems*, Prentice-Hall, Englewood Cliffs, NJ (1991).
2. W. Tiedemann and J. Newman, in *Battery Design and Optimization*, S. Gross, Editor, PV 79-1, p. 23, The Electrochemical Society Proceedings Series, Pennington, NJ (1979).
3. W. G. Sunu, in *Electrochemical Cell Design*, R. E. White, Editor, p. 357, Plenum Press, New York (1984).
4. H. Gu, T. V. Nguyen, and R. E. White, *J. Electrochem. Soc.*, **134**, 2953 (1987).
5. W. B. Gu, C. Y. Wang, and B. Y. Liaw, *J. Electrochem. Soc.*, **144**, 2053 (1997).
6. D. Fan and R. E. White, *J. Electrochem. Soc.*, **138**, 17 (1991).
7. D. Fan and R. E. White, *J. Electrochem. Soc.*, **138**, 2952 (1991).
8. P. De Vidts and R. E. White, *J. Electrochem. Soc.*, **142**, 1509 (1995).
9. B. V. Ratnakumar, P. Timmerman, C. Sanchez, S. D. Stefano, and G. Halpert, *J. Electrochem. Soc.*, **143**, 803 (1996).
10. B. Paxton and J. Newman, *J. Electrochem. Soc.*, **144**, 3818 (1997).
11. T. F. Fuller, M. Doyle, and J. Newman, *J. Electrochem. Soc.*, **141**, 1 (1994).
12. P. De Vidts, J. Delgado, and R. E. White, *J. Electrochem. Soc.*, **142**, 4006 (1995).
13. J. K. Heikonen, K. Vuorilehto, and T. Noponen, *J. Electrochem. Soc.*, **143**, 3972 (1996).
14. C. Y. Yuh and J. R. Selman, *J. Electrochem. Soc.*, **131**, 2062 (1984).
15. J. A. Prins-Jansen, J. D. Fehribach, K. Hemmes, and J. H. W. De Wit, *J. Electrochem. Soc.*, **143**, 1617 (1996).
16. T. F. Fuller and J. Newman, *J. Electrochem. Soc.*, **140**, 1218 (1993).
17. T. V. Nguyen and R. E. White, *J. Electrochem. Soc.*, **140**, 2178 (1993).
18. J. Bouet, F. Richard, and P. Blanchard, in *Nickel Hydroxide Electrodes,* D. A. Corrigan and A. H. Zimmerman, Editors, PV 90-4, p. 260, The Electrochemical Society Proceedings Series, Pennington, NJ (1990).
19. T. F. Fuller and J. Newman, in *Modern Aspects of Electrochemistry*, Vol. 27, R. E. White, J. O'M. Bockris, and B. E. conway, Editors, p. 359, Plenum Press, New York (1995).
20. R. M. Lafollette and D. N. Bennion, *J. Electrochem. Soc.*, **137**, 3701 (1990).
21. K. C. Tsaur and R. Pollard, *J. Electrochem. Soc.*, **133**, 2296 (1986).
22. D. M. Bernardi, *J. Electrochem. Soc.*, **137**, 1670 (1990).
23. J. Newman and W. Tiedemann, *AIChE J.*, **21**, 25 (1975).
24. M. M. Saleh, J. W. Weidner, and B. G. Ateya, *J. Electrochem. Soc.*, **142**, 4113 (1995).
25. G. Savaskan, T. Huh, and J. W. Evans, *J. Appl. Electrochem.*, **22**, 909 (1992).
26. J. C. Slattery, *Momentum, Energy and Mass Transfer in Continua*, McGraw-Hill, New York (1981).
27. J. C. Slattery, *AIChE J.*, **15**, 866 (1969).
28. S. Whitaker, *Ind. Eng. Chem.*, **61**, 14 (1969).
29. M. Hassanizadeh and W. G. Gray, *Adv. Water Resour.*, **3**, 25 (1980).
30. J. Bear and J-M. Buchlin, *Modeling and Applications of Transport Phenomena in Porous Media,* Kluwer, Boston, MA (1991).
31. P. De Vidts and R. E. White, *J. Electrochem. Soc.*, **144**, 1343 (1997).
32. C. Y. Wang and C. Beckermann, *Metall. Mater. Trans. A*, **27A**, 2754 (1996).
33. H. Brenner and D. A. Edwards, *Macrotransport Processes,* Butterworth Scientific, London (1993).
34. S. Whitaker, *Transp. in Porous Media*, **1**, 105 (1986).
35. E. E. Underwood, *Quantitative Stereology*, Addison-Wesley Publishing Co., Reading, MA (1970).
36. S. P. Marsh and M. E. Glicksman, in *Proceedings of Modeling of Casting, Welding and Advanced Solidification Processes VI*, T. S. Piwonka, V. Voller, and L. Katgerman, Editors, p. 55, The Minerals, Metals & Materials Society, TMS, Warrendale, PA (1993).
37. K. Petrov, A. A. Rostami, A. Visintin, and S. Srinivasan, *J. Electrochem. Soc.*, **141**, 1747 (1994).
38. M. N. Ozisik, *Heat Conduction*, Chap. 9, John Wiley & Sons, New York (1993).
39. M. Doyle, T. F. Fuller, and J. Newman, *J. Electrochem. Soc.*, **140**, 1526 (1993).
40. M. Doyle, J. Newman, A. S. Gozdz, C. N. Schmutz, and J-M. Tarascon, *J. Electrochem. Soc.*, **143**, 1890 (1996).
41. C. Wagner, *J. Electrochem. Soc.*, **98**, 116 (1951).
42. M. Z. A. Munshi and B. B. Owens, *Solid State Ionics*, **38**, 87 (1990).
43. W. B. Gu, C. Y. Wang, and B. Y. Liaw, *J. Electrochem. Soc.*, **145**, 3418 (1998).